A new method to measure electron density and effective atomic number using dual-energy CT images

2016 Phys. Med. Biol. 61 265

(http://iopscience.iop.org/0031-9155/61/1/265)

IOP Publishing | Institute of Physics and Engineering in Medicine Physics in Medicine & Biology

Phys. Med. Biol. **61** (2016) 265–279 doi:10.1088/0031-9155/61/1/265

A new method to measure electron density and effective atomic number using dual-energy CT images

Luis Isaac Ramos Garcia[1], **José Fernando Pérez Azorin**[2] **and Julio F Almansa**[3]

[1] Department of Oncology, Clínica Universidad de Navarra, University of Navarra, Av Pio XII s/n, Pamplona, Navarre, Spain
[2] Medical Physics Department, Hospital Universitario de Cruces, Plz. Cruces, Barakaldo, Spain
[3] Medical Physics Department, Hospital Universitario Virgen de las Nieves, Av de las Fuerzas Armadas, Granada, Spain

E-mail: liramos@unav.es

Received 16 June 2015
Accepted for publication 9 November 2015
Published 9 December 2015

Abstract

The purpose of this work is to present a new method to extract the electron density (ρ_e) and the effective atomic number (Z_{eff}) from dual-energy CT images, based on a Karhunen-Loeve expansion (KLE) of the atomic cross section per electron. This method was used to calibrate a Siemens Definition CT using the CIRS phantom. The predicted electron density and effective atomic number using 80 kVp and 140 kVp were compared with a calibration phantom and an independent set of samples. The mean absolute deviations between the theoretical and calculated values for all the samples were 1.7 % $\pm$ 0.1 % for $\rho_e$and 4.1 % $\pm$ 0.3 % for Z_{eff}. Finally, these results were compared with other stoichiometric method. The application of the KLE to represent the atomic cross section per electron is a promising method for calculating ρ_e and Z_{eff} using dual-energy CT images.

Keywords: tissue characterization, dual-energy CT, electron density, effective atomic number

(Some figures may appear in colour only in the online journal)

1. Introduction

With the continuous improvement in computation capabilities, the Monte Carlo (MC) simulation has become an alternative for dosimetric calculations. The accuracy of MC dose calculation relies on the knowledge of compositional data of patient tissues (Seco and Evans 2006, Landry *et al* 2011a).

Conventional single-energy CT images cannot provide this information because they only give an estimate of electron density (Schneider *et al* 1996, Schneider *et al* 2000). An alternative is dual-energy CT, where the properties of the tissue, electron density (ρ_e) and effective atomic number (Z_{eff}) are calculated when the tissue is exposed to different energies of x-rays (Heismann *et al* 2003, Bazalova *et al* 2008a, 2008b, Zhang *et al* 2008, Landry *et al* 2011b, Landry *et al* 2013, Bourque *et al* 2014).

There are currently three major algorithms for post-processing dual-energy CT images (Williamson *et al* 2006, Bourque *et al* 2014); the main difference between them is the model used to represent the attenuation coefficient.

The basis vector model (Heismann *et al* 2003, Williamson *et al* 2006, Liu *et al* 2009) assumes that any attenuation coefficient can be described as a linear combination of two basis attenuation coefficients, corresponding to the basis substances:

$$\mu_{\text{tissue}}(E) = a_{\text{tissue}}\left[\frac{\mu(E)}{\rho}\right]_a + b_{\text{tissue}}\left[\frac{\mu(E)}{\rho}\right]_b \tag{1}$$

Where $\left[\frac{\mu(E)}{\rho}\right]_{a,b}$ are the mass attenuation coefficients of the basis substances a and b, and the parameters a_{tissue} and b_{tissue} are their corresponding coefficients.

When equation (1) is applied to dual-energy CT, the coefficients a_{tissue} and b_{tissue} are obtained and the quantities of interest can be calculated (Williamson *et al* 2006), e.g. ρ_e, Z_{eff}, energy absorption coefficients, etc.

For the parametric model, the attenuation coefficients are modeled as the sum of the main interaction processes at energies of interest, i.e. photoelectric effect, Compton effect and Rayleigh scattering effect (Heismann *et al* 2003, Williamson *et al* 2006, Landry *et al* 2013):

$$\mu_{\text{tissue}}(E) = \rho_e\,[f_{\text{ph}}(E)Z_{\text{eff}}^{k_{\text{ph}}} + \sigma_{\text{KN}}(E) + f_{\text{Ry}}(E)Z_{\text{eff}}^{k_{\text{Ry}}}] \tag{2}$$

Where σ_{KN} is the Klein-Nishima cross section and $f_{\{\text{ph, Ry}\}}$, $k_{\{\text{ph, Ry}\}}$ are energy dependent functions and exponents associated with photoelectric (ph) and Rayleigh (Ry) effects, respectively.

This model assumes that the atomic cross section for the photoelectric and Rayleigh effects can be expressed as a power function of the atomic number (Jackson and Hawkes 1981) and the effective atomic numbers for these two interactions are approximately equal and independent of energy (Williamson *et al* 2006).

Midgley (Midgley 2004) expands the attenuation coefficients using natural powers of Z_{eff}:

$$\mu_{\text{tissue}}(E) = \sum_{\text{i}=0}^{N} S_{\text{i}}(E) M_{\text{i,tissue}} \tag{3}$$

In the above equation, the number of terms in the expansion N should be at least four (Midgley 2004), $S_{\text{i}}(E)$ is an energy dependent function, and $M_{\text{i,tissue}}$ are the characteristic functions of the tissue composition:

$$M_{\text{i,tissue}} = N_a \rho \sum_{Z} \frac{w(Z)}{A(Z)} Z^{\text{i}} \tag{4}$$

In equation (4), N_a is the Avogadro's number, ρ is the mass density, $A(Z)$ is the mass number and $w(Z)$ is the mass fraction of the element with atomic number Z.

This expansion is used by Bourque *et al* (Bourque *et al* 2014) to perform a stoichiometric calibration of a dual-energy CT.

In any case, a necessary condition for a useful parameterization (without the knowledge of the x-ray spectrum and the sensitivity of the detectors in detail) is the separability between energy and atomic number (Williamson *et al* 2006), i.e. the model should have the form:

$$\mu(E) = \sum_{i=0}^{N} F_i(Z,\rho) G_i(E) \tag{5}$$

In equation (5) $F_i(Z,\rho)$ depends only on the atomic number and density and $G_i(E)$ depends only on the energy.

This representation is not unique and any set of linear independent functions $\{F_i(Z,\rho)\}$ gives a new representation. There is a mathematical method to calculate an optimal representation as in equation (5), known as proper orthogonal decomposition or Karhunen-Loeve expansion (KLE) (Hyvärinen *et al* 2004, Buljak 2011). The optimal representation means that, given the order N and in the least square sense, there is no other expansion like (5) better than the KLE (Buljak 2011).

The KLE is defined for continuous functions, but for discrete data, this representation is directly related to the principal component analysis and the singular value decomposition of matrices (Buljak 2011).

The objective of this study is to propose a stoichiometric calibration of a dual-energy CT based on the Karhunen-Loeve expansion. This method was proposed by Bornefalk (Bornefalk 2012), but has not been implemented, as far as the authors are aware.

2. Methods and materials

2.1. Proper orthogonal decomposition of the atomic cross section per electron

From a practical point of view, it is better to work with the atomic cross section per electron or the quotient between the attenuation coefficient and electron density because the electron density is explicitly taken into account and the range of variation of the cross sections is reduced by at least one order of magnitude (Midgley 2004). The relationship between both is direct:

$$\left(\frac{\mu}{\rho_e}\right) = \frac{\sigma_a}{Z} = \frac{1}{N_a}\frac{A(Z)}{Z}\left(\frac{\mu}{\rho}\right) \tag{6}$$

In equation (6), ρ_e is the electron density and σ_a is the atomic cross section.

The KLE represents the variability from the mean value of any function as a sum of weighted, orthogonal basis functions. Using the mean value in Z, the KLE of the atomic cross section per electron gives:

$$\left(\frac{\mu}{\rho_e}\right) = g_0(E) + \sum_{i=1}^{N} f_i(Z) g_i(E) \tag{7}$$

Where $g_0(E)$ is the mean value of the atomic cross section per electron, and $f_i(Z)$ and $g_i(E)$ are the functions of the KLE.

$$g_0(E) = \frac{1}{n}\sum_{Z=1}^{n}\left(\frac{\mu}{\rho_e}\right)(Z,E) \tag{8}$$

The orthogonal basis $f_i(Z)$ can be calculated by solving the following eigenvalue problem (Hyvärinen *et al* 2004, Buljak 2011):

$$Cf_i(Z) = \lambda_i f_i(Z) \tag{9}$$

Where, in equation (9), C is a positive definite matrix associated with the autocorrelation:

$$C(Z_i, Z_j) = \frac{1}{n}\int_0^{E_{max}} \left[\frac{\mu(Z_i,E)}{\rho_{e,i}} - g_0(E)\right]\left[\frac{\mu(Z_j,E)}{\rho_{e,j}} - g_0(E)\right] dE \tag{10}$$

In equation (9), λ_i is the eigenvalue associated with the basis function $f_i(Z)$. Its value determines the importance of this function in the expansion.

After the expansion and from equation (7), we calculate the attenuation coefficient of composed tissues using the mixed rule and the relation between electron and mass densities (Jackson and Hawkes 1981):

$$\mu_{tissue}(Z,E) = \rho_{tissue} N_a \sum_Z \frac{w(Z)}{A(Z)} \sigma_a(Z,E) \tag{11}$$

$$\rho_e = \rho_{tissue} N_a \sum_Z w(Z) \frac{Z}{A(Z)} \tag{12}$$

Hence,

$$\mu_{tissue} = g_0(E)\rho_e + \rho_{tissue} N_a \sum_i g_i(E) \sum_Z \frac{w(Z)}{A(Z)} Z f_i(Z) \tag{13}$$

When the density relative to water is introduced, the equation (13) becomes:

$$\begin{aligned}\mu_{tissue} &= [g_0(E)\rho_e^w]\,\rho_e^{tissue,w} + \rho^{tissue,w}\frac{2A_H + A_O}{2Z_H + Z_O}\sum_i [g_i(E)\rho_e^w]\sum_Z \frac{w(Z)}{A(Z)} Z f_i(Z) = \\ &= [g_0(E)\rho_e^w]\,\rho_e^{tissue,w} + \sum_i [g_i(E)\rho_e^w]\, M_{i,tissue}\end{aligned} \tag{14}$$

In equation (14), A_H, Z_H A_O and Z_O are the mass and atomic numbers of the hydrogen (H) and oxygen (O) respectively, ρ_e^w is the electron density of water, $\rho_e^{tissue,w}$ and $\rho^{tissue,w}$ are the tissue electron and mass densities relative to water and $M_{i,tissue}$ is a new set of functions defined as:

$$M_{i,tissue} = \rho^{tissue,w}\frac{2A_H + A_O}{2Z_H + Z_O}\sum_Z \frac{w(Z)}{A(Z)} Z f_i(Z) \tag{15}$$

2.2. Data used in the expansion

Attenuation coefficients supplied by NIST were used. These coefficients were obtained using the WinXCOM program (Gerward *et al* 2004). Only elements with biological interest were taken into account (Z between Hydrogen and Calcium). The energies ranged between 20 and 10^3 keV (Williamson *et al* 2006). Within this range, the values were interpolated using the natural logarithm and cubic splines. To calculate the correlation in equation (10), the Gauss-Legendre quadrature was used.

Assuming that the attenuation coefficient and the atomic number are independent variables and both are normally distributed, the uncertainties of the expansion were calculated by simulation. The variability in the attenuation coefficients were selected as 2% (Hubbell 1999) and

the atomic weights and their uncertainties were taken from the 2011 UIPAC technical report (Wieser *et al* 2013).

2.3. Calibration of the CT

In computed tomography, the relationship between the Hounsfield units (HU) and the relative attenuation coefficient is linear:

$$\mu_{\text{water}}^{\text{tissue}} = \frac{\text{HU}}{\alpha_{\text{HU}}} + \beta_{\text{HU}} \tag{16}$$

Where $\mu_{\text{water}}^{\text{tissue}}$ is the quotient between the effective attenuation coefficients of tissue and water. Ideally, $\alpha_{\text{HU}} = 1000$ and $\beta_{\text{HU}} = 1$; however, in practice, slight differences are expected (Williamson *et al* 2006).

Using equation (14), the effective attenuation coefficients normalized to water can be expressed as:

$$\mu_{\text{water}}^{\text{tissue}} = \frac{g_0}{g_0 + \sum_{\text{i}} g_{\text{i}} M_{\text{i,water}}} \rho_{\text{e}}^{\text{tissue},w} + \sum_{\text{i}} \frac{g_{\text{i}}}{g_0 + \sum_{\text{i}} g_{\text{i}} M_{\text{i,water}}} M_{\text{i,tissue}} \tag{17}$$

Where the functions g_{i} are the mean values of the $g_{\text{i}}(E)\rho_{\text{e}}^{w}$ functions weighted over the x-ray spectra and detector sensitivity.

Finally, using equations (16) and (17), and defining the parameters C_0, C_ρ and $C_{M_{\text{i}}}$ the relationship between the HU, the ρ_{e} and the $\text{M}_{\text{i,tissue}}$ functions is:

$$\text{HU} = C_0 + C_\rho \rho_{\text{e}}^{\text{tissue},w} + \sum_{\text{i}} \text{C}_{M_{\text{i}}} M_{\text{i,tissue}} \tag{18}$$

Only one term in the KLE gives an accurate representation of the atomic cross section per electron (see section 3.1). Taking this fact into account:

$$\text{HU} = C_0 + C_\rho \rho_{\text{e}}^{\text{tissue},w} + C_{M_{\text{I}}} M_{\text{1,tissue}} \tag{19}$$

Through equation (19), the CT can be calibrated by means of the least squares estimator for the parameters C_0, C_ρ and $C_{M_{\text{I}}}$ using samples of known composition.

The phantom used for the calibration was the CIRS phantom model 62M, the composition and sample densities of which were taken from Pelmer (Pemler *et al* 2001). These data were used to calculate $\rho_{\text{e}}^{\text{tissue},w}$ and $M_{\text{i,tissue}}$ using equations (12) and (15). The uncertainties in both quantities were not taken into account in the CT calibration because there is no estimate of the uncertainties of the compositions.

For the CIRS phantom, there is more than one sample for the same material. For each sample of the same material, a circular ROI was used to get the mean HU of the pixels inside. Finally, all the averages of the samples of the same material were used to calculate the mean and standard deviation of the HU associated with the material.

To obtain the calibration curve, a linear weighted regression (De Levie 2012) was performed between the HU and the pair $\rho_{\text{e}}^{\text{tissue},w}$, $M_{\text{i,tissue}}$

To check the accuracy of our calibration, this calibration was applied to a set of independent samples of known composition, which we placed in an in-house phantom. This phantom was made in our institution using PTW-RW3 solid water with the addition of different liquid substances with known compositions (figure 1). The compositions of the substances used are listed in table 1. One of the most interesting materials is the silicon oil which has a lower

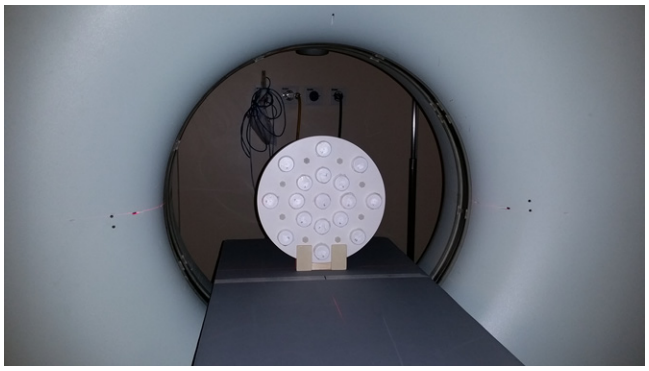

Figure 1. Detail of the phantom used to hold the liquid substances used to verify the calibration.

density than water but a larger Z_{eff} (and therefore a larger inferred HU value) due to the presence of silicon in the composition.

The images were taken using a Siemens Definition CT at 80 and 140 kVp. Two scans were used to take the images for each kVp. The parameters of the scanning protocol are listed in table 2.

2.4. Calculation of ρ_e and Z_{eff}

The calculation of the pair $\rho_e^{\text{tissue},w}$, $M_{1,\text{tissue}}$ is made by solving the linear system of equations obtained by considering the highest and lowest tube voltage in equation (19):

$$\rho_e^{\text{tissue},w} = \frac{C_{M_1}^{\text{L}}(\text{HU}^{\text{H}} - C_0^{\text{H}}) - C_{M_1}^{\text{H}}(\text{HU}^{\text{L}} - C_0^{\text{L}})}{C_{M_1}^{\text{L}} C_\rho^{\text{H}} - C_{M_1}^{\text{H}} C_\rho^{\text{L}}} \tag{20}$$

$$M_{1,\text{tissue}} = \frac{C_\rho^{\text{L}}(\text{HU}^{\text{H}} - C_0^{\text{H}}) - C_\rho^{\text{H}}(\text{HU}^{\text{L}} - C_0^{\text{L}})}{C_{M_1}^{\text{H}} C_\rho^{\text{L}} - C_{M_1}^{\text{L}} C_\rho^{\text{H}}} \tag{21}$$

In equations (20) and (21), the superscript L and H refer to low and high voltage of the tube, respectively.

The effective atomic number is calculated by considering that for an element, equation (15) is:

$$M_{1,\text{tissue}} = \rho^{\text{tissue},w} \frac{2A_{\text{H}} + A_{\text{O}}}{2Z_{\text{H}} + Z_{\text{O}}} \frac{Z_{\text{eff}}}{A(Z_{\text{eff}})} f_1(Z_{\text{eff}}) = \rho_e^{\text{tissue},w} f_1(Z_{\text{eff}}) \tag{22}$$

And hence,

$$Z_{\text{eff}} = f_1^{-1}\left(\frac{M_{1,\text{tissue}}}{\rho_e^{\text{tissue},w}}\right) \tag{23}$$

Equation (23) can be expressed in terms of the calibration parameters and HU directly; using the dual-energy ratio (Bourque *et al* 2014):

$$\Gamma = \frac{\text{HU}^{\text{L}} - \text{C}_0^{\text{L}}}{\text{HU}^{\text{H}} - \text{C}_0^{\text{H}}} \tag{24}$$

Table 1. Mass density and composition of the samples used to test the calibration.

	ρ	H	C	N	O	F	Na	Al	Si	P	Cl	K	Ca
	g cm^{-3}	1	6	7	8	9	11	13	14	15	17	19	20
CH_3–CHOH–CH_3 Isopropyl 2-propanol	0.787	0.134	0.599	0.000	0.267	0.000	0.000	0.000	0.000	0.000	0.000	0.000	0.000
CH_3–CHOH–CH_2OH 1,2 Propanediol	1.040	0.106	0.472	0.000	0.422	0.000	0.000	0.000	0.000	0.000	0.000	0.000	0.000
CH_3–$(CH_2)_3$–CH_2OH N-amyl alcohol, 1-pentanol	0.810	0.137	0.674	0.000	0.189	0.000	0.000	0.000	0.000	0.000	0.000	0.000	0.000
$CH_3(CH_2)_3OH$ Butanol	0.810	0.136	0.642	0.000	0.223	0.000	0.000	0.000	0.000	0.000	0.000	0.000	0.000
CH_3OH Methanol	0.792	0.126	0.374	0.000	0.500	0.000	0.000	0.000	0.000	0.000	0.000	0.000	0.000
(–$Si(CH_3)_2O$–)n Silicon oil	0.987	0.082	0.324	0.000	0.216	0.000	0.000	0.000	0.379	0.000	0.000	0.000	0.000
NaF Sodium fluoride	1.026	0.110	0.000	0.000	0.871	0.009	0.011	0.000	0.000	0.000	0.000	0.000	0.000
$Al(NO_3)_3$ $9H_2O$ Aluminum nitrate 9-hydrate	1.016	0.110	0.000	0.003	0.885	0.000	0.000	0.002	0.000	0.000	0.000	0.000	0.000
Na_2SiO_3 sodium silicate	1.365	0.000	0.000	0.000	0.393	0.000	0.377	0.000	0.230	0.000	0.000	0.000	0.000
Na_2HPO_4 Dibasic sodium phosphate	1.043	0.107	0.000	0.000	0.867	0.000	0.015	0.000	0.000	0.010	0.000	0.000	0.000
KCl potassium chloride	1.017	0.109	0.000	0.000	0.862	0.000	0.000	0.000	0.000	0.000	0.014	0.015	0.000
$CaCl_2$ $2H_2O$ Calcium chloride 2-hydrate	1.221	0.084	0.000	0.000	0.670	0.000	0.000	0.000	0.000	0.000	0.157	0.000	0.089
$C_3H_8O_3$ Glycerol	1.259	0.088	0.391	0.000	0.521	0.000	0.000	0.000	0.000	0.000	0.000	0.000	0.000
CH_3COCH_3 Acetone	0.790	0.104	0.620	0.000	0.275	0.000	0.000	0.000	0.000	0.000	0.000	0.000	0.000
$CH_3COOC_2H_5$ Ethyl acetate	0.902	0.092	0.544	0.000	0.365	0.000	0.000	0.000	0.000	0.000	0.000	0.000	0.000
$CH_3CHOHCH_3$ 2-propanol	0.785	0.134	0.598	0.000	0.268	0.000	0.000	0.000	0.000	0.000	0.000	0.000	0.000
$C_6H_5CH_3$ Toluene	0.870	0.088	0.912	0.000	0.000	0.000	0.000	0.000	0.000	0.000	0.000	0.000	0.000
CH_3CH_2OH Ethanol	0.790	0.131	0.520	0.000	0.349	0.000	0.000	0.000	0.000	0.000	0.000	0.000	0.000
C_4H_8O Ethyl methyl ketone	0.805	0.112	0.665	0.000	0.224	0.000	0.000	0.000	0.000	0.000	0.000	0.000	0.000

Table 2. Parameters of the scanning protocol.

Mode	Axial
Pitch	N/A
kVp	80–140
mA	320
Rotation time (s)	1
mAs	320
FOV (cm)	50
Reconstruction diameter (cm)	50
Slice thickness (mm)	1.2
Convolution kernel	H31s

Using (20)–(24) Z_{eff} can be calculated as follows:

$$Z_{\text{eff}} = f_1^{-1}\left(\frac{C_\rho^{\text{H}}\,\Gamma - \text{C}_\rho^{\text{L}}}{\text{C}_{M_1}^{\text{L}} - \text{C}_{M_1}^{\text{H}}\Gamma}\right) \tag{25}$$

Equation (20) implies a linear relation between ρ_e and $\text{HU}^{\{\text{H,L}\}}$, exactly in the same manner as the equation proposed by Saito (Saito 2011, 2012, Tsukihara *et al* 2013, Saito and Tsukihara 2014, Saito 2015, Tsukihara *et al* 2015). In fact, taking the following transformations:

$$a = 10^3 \frac{C_{M_1}^{\text{L}} - C_{M_1}^{\text{H}}}{C_{M_1}^{\text{L}} C_\rho^{\text{H}} - C_{M_1}^{\text{H}} C_\rho^{\text{L}}} \tag{26}$$

$$b = \frac{C_0^{\text{L}} C_{M_1}^{\text{H}} - C_0^{\text{H}} C_{M_1}^{\text{L}}}{C_{M_1}^{\text{L}} C_\rho^{\text{H}} - C_{M_1}^{\text{H}} C_\rho^{\text{L}}} \tag{27}$$

$$\alpha = \frac{C_{M_1}^{\text{H}}}{C_{M_1}^{\text{L}} - C_{M_1}^{\text{H}}} \tag{28}$$

The relation between the dual energy subtraction ΔHU and ρ_e is reproduced:

$$\rho_e = \frac{a}{10^3}(1+\alpha)\text{HU}^{\text{H}} - \frac{a}{10^3}\alpha\text{HU}^{\text{L}} + b = \frac{a}{10^3}\Delta\text{HU} + b \tag{29}$$

2.5. Comparison with Bourque's method

To compare the method presented in this work with other methods, the method of Bourque *et al* (Bourque *et al* 2014) was chosen, since this is the latest published method. For comparison purposes, the Z_{eff} values of the calibration and test samples were calculated using equations (12), (15) and (23).

The reduced Hounsfield units were calculated in the same manner as that defined by the author in their work:

$$u_{\text{L,H}} = \frac{\text{HU}_{\text{L,H}} + 1000}{1000} \tag{30}$$

Finally, the reduced Hounsfield units were fitted to polynomial functions to obtain the calibration functions:

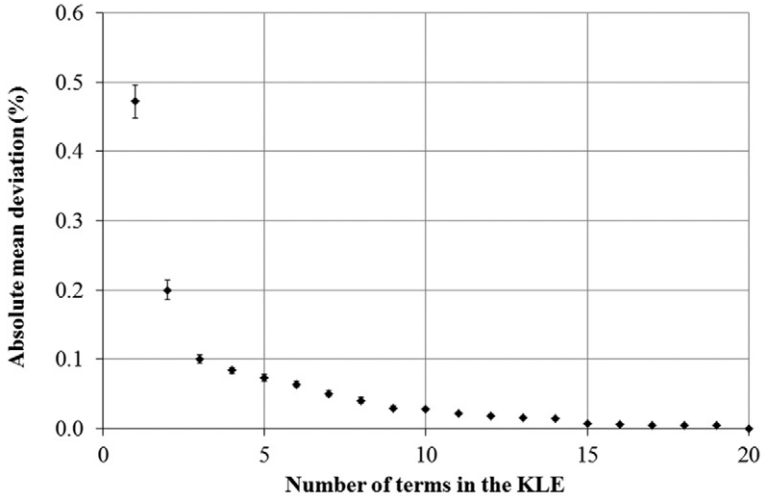

Figure 2. Absolute error in (%) versus the number of terms N in the KLE approximation.

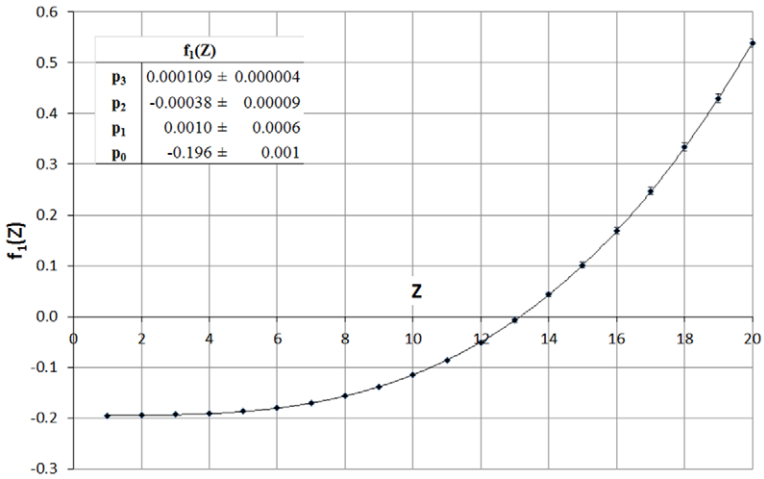

Figure 3. Eigenfunction $f_1(Z)$. The values of the function are approximated using a third order polynomial; the parameters of the polynomial fit are shown in the figure and the uncertainties are shown with $k = 1$ as coverage factor.

$$Z_{\text{eff}} = f\left(\frac{u_{\text{L}}}{u_{\text{H}}}\right) \tag{31}$$

$$\frac{u_{\text{L,H}}}{\rho_{\text{e}}} = g_{\text{L,H}}(Z_{\text{eff}}) \tag{32}$$

As before, the CIRS phantom model 62M was employed for calibration and these results were subsequently used in the test materials.

Table 3. Results for the calibration of the two tube voltages considered.

80 kVp				140 kVp			
$C_0 =$	−959	±	16	$C_0 =$	−1023	±	8
$C_\rho =$	1558	±	92	$C_\rho =$	1295	±	10
$C_{M_1} =$	3731	±	563	$C_{M_1} =$	1652	±	60

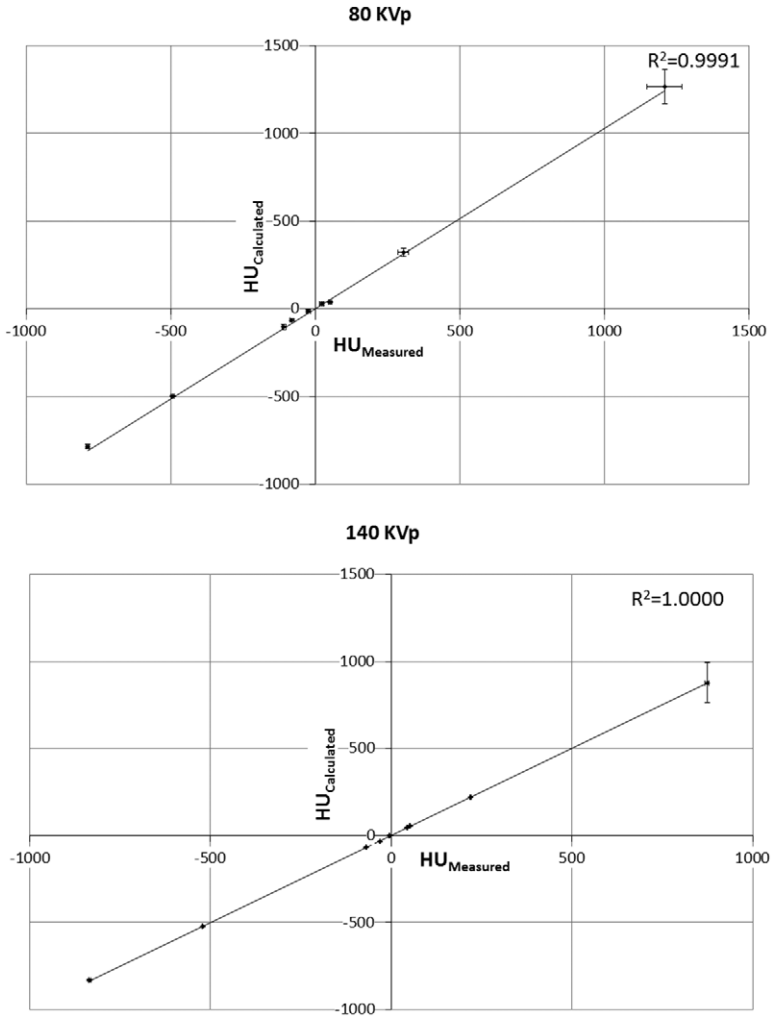

Figure 4. HU measured using the images given by the CT versus the HU calculated using the parameters of the calibration in table 3. The line represents a linear regression fit forced to pass through the origin. In both cases, the correlation coefficients of these fits are greater than 0.999.

2.6. Statistical methods used in comparisons

In this study, we assume that the mean relative differences follow a normal distribution. Therefore, t Student test was used to compare these means. However, for analyzing the significance of absolute deviations, the normal distribution hypothesis is not strictly true, so the

Table 4. Results for ρ_e and Z_{eff} and their relative differences between data obtained using the method presented and their theoretical values for the CIRS 62M phantom.

	$\rho_{\text{e}}^{\text{tissuse},w}$			Z_{eff}		
	Theoretical	Calculated	Δ (%)	Theoretical	Calculated	Δ (%)
Breast 50/50	0.98	1.00 ± 0.03	−2.0	6.83	5.80 ± 0.05	15.0
Adipose	0.95	0.96 ± 0.04	−0.5	6.38	6.07 ± 0.06	5.0
Trabecular bone 200 mg/cc HA	1.12	1.13 ± 0.05	−1.2	10.18	9.88 ± 0.04	3.0
Dense bone 800 mg/cc HA	1.51	1.5 ± 0.4	−2.5	12.67	12.2 ± 0.4	3.8
Liver	1.05	1.04 ± 0.03	1.4	7.50	7.98 ± 0.03	−6.4
Lung (inhale)	0.19	0.19 ± 0.03	2.6	6.83	7.0 ± 0.3	−2.7
Lung (exhale)	0.49	0.49 ± 0.02	0.0	7.41	7.55 ± 0.03	−1.8
Muscle	1.04	1.05 ± 0.03	−0.5	7.51	7.27 ± 0.03	3.1
Plastic Water-LR	1.00	1.00 ± 0.03	−0.1	7.51	7.26 ± 0.03	3.3
Relative differences (%)		Mean =	−0.3		Mean =	2.3
		SD =	1.8		SD =	6.9
Absolute differences (%)		Mean =	1.2		Mean =	4.9
		SD =	1.0		SD =	4.0

Wilcoxon-Mann-Whitney test was used. In all these tests, 0.05 was taken as the threshold for statistical significance.

3. Results

3.1. KL expansion of the atomic cross section per electron

Figure 2 shows the absolute error in (%) of the cross section per electron calculated using the KLE as the numbers of terms in the approximation increase.

As can be observed in figure 2, as the number of terms in the expansion increases, the errors fall to zero. However, with the first term alone, the mean absolute error is 0.47 % with a standard deviation of 0.8 %.

Figure 3 shows the eigenfunction $f_1(Z)$. The values of this function can be accurately approximated with a third order polynomial.

3.2. CT calibration

Table 3 shows the calibration for 80 and 140 kVp. For the lower energy, C_0 is beyond two standard deviations from the ideal value of −1000.

Figure 4 represents the HU measured versus the HU calculated using the parameters in table 3. A good correlation is found for the two energies ($R^2 > 0.999$).

3.3. Calculation of ρ_{e} and Z_{eff}

Tables 4 and 5 show the differences between the theoretical and calculated values for the samples in the CIRS and test phantoms respectively.

Table 5. Results for $\rho_e$and Z_{eff} and their relative differences between data obtained using the method presented and their theoretical values for the test phantom.

	$\rho_e^{tissue,w}$			Z_{eff}		
	Theoretical	Calculated	Δ (%)	Theoretical	Calculated	Δ (%)
CH_3–CHOH–CH_3 Isopropyl 2-propanol	0.80	0.82 ± 0.02	−1.7	6.24	5.94 ± 0.05	4.7
CH_3–CHOH–CH_2OH 1,2 Propanediol	1.03	1.04 ± 0.03	−0.7	6.66	7.18 ± 0.03	−7.7
CH_3–$(CH_2)_3$–CH_2OH N-amyl alcohol 1-pentanol	0.83	0.85 ± 0.02	2.7	6.04	6.02 ± 0.05	0.2
CH_3–CH_2–OH Ethanol	0.82	0.84 ± 0.02	−2.1	6.45	6.30 ± 0.04	2.3
$CH_3(CH_2)_3OH$ Butanol	0.83	0.85 ± 0.02	−2.3	6.13	5.79 ± 0.05	5.5
CH_3OH Methanol	0.80	0.82 ± 0.02	2.0	6.76	6.79 ± 0.04	−0.4
(–$Si(CH_3)_2O$–)n Silicon oil	0.96	0.97 ± 0.03	1.0	10.55	10.83 ± 0.03	−2.7
NaF Sodium fluoride	1.02	1.03 ± 0.04	0.9	7.54	7.79 ± 0.03	−3.3
$Al(NO_3)_3 9H_2O$ Aluminum Nitrate 9-hydrae	1.01	1.03 ± 0.03	−1.3	7.50	7.80 ± 0.03	−4.0
Na_2SiO_3 Sodium Silicate	1.21	1.29 ± 0.04	6.7	11.05	10.39 ± 0.03	6.0
Na_2HPO_4 Dibasic sodium phosphate	1.04	1.05 ± 0.03	1.2	7.73	8.05 ± 0.03	−4.1
KCl Potassium chloride	1.01	1.03 ± 0.02	1.3	8.33	8.34 ± 0.03	−0.2
$CaCl_2 2H_2O$ Calcium chloride 2-hydrate	1.18	1.21 ± 0.06	2.5	12.05	12.11 ± 0.04	−0.5
$C_3H_8O_3$ Glycerol	1.23	1.25 ± 0.06	−1.9	6.92	7.26 ± 0.03	−4.9
CH_3COCH_3 Acetone	0.78	0.80 ± 0.02	−1.5	6.35	6.08 ± 0.05	4.3
$CH_3COOC_2H_5$ Ethyl Acetate	0.89	0.89 ± 0.02	−0.6	6.59	6.83 ± 0.04	−3.6
$CH_3CHOHCH_3$ 2-propanol	0.80	0.82 ± 0.02	3.0	6.24	6.04 ± 0.05	3.2
$C_6H_5CH_3$ Toluene	0.85	0.86 ± 0.02	0.7	5.69	6.11 ± 0.04	−7.5
C_4H_8O Ethyl methyl ketone	0.80	0.82 ± 0.02	−2.0	6.20	5.89 ± 0.05	5.1
Relative differences (%)		Mean = 0.4			Mean = −0.4	
		SD = 2.3			SD = 4.4	
Absolute differences (%)		Mean = 1.9			Mean = 3.7	
		SD = 1.4			SD = 2.3	

The theoretical ρ_e and Z_{eff} were calculated using the mass composition and equations (12), (15) and (23). The experimental quantities are derived from the HU and calibration parameters for 80 kVp and 140 kVp using equations (20) and (25).

For the CIRS materials, the mean relative deviation between theoretical and experimental quantities was −0.3 % ± 0.5 % for ρ_e and 2.3 % ± 0.5 % for Z_{eff}. These differences are not statically different from zero ($p_{t,\rho_e} = 0.572$; $p_{t,Z_{eff}} = 0.252$).

For the test materials, the relative deviations were 0.4 % ± 0.3 % for electron density and −0.4 % ± 0.5 % for Z_{eff}. Again, the differences are not statistically different from zero ($p_{t,\rho_e} = 0.449$; $p_{t,Z_{eff}} = 0.697$).

Table 6. Descriptive statistics for the results of the stoichiometric methods.

		KLE		Bourque	
		$\rho_e^{tissuse,w}$	Z_{eff}	$\rho_e^{tissuse,w}$	Z_{eff}
Relative differences (%)	Mean =	0.2	0.3	−1.1	−8.1
	SD =	2.2	5.2	9.6	22.9
	Max =	6.7	15.0	32.4	19.1
	Min =	−2.5	−7.7	−21.5	−105.7
Absolute differences (%)	Mean =	1.7	4.1	5.4	13.2
	SD =	1.3	2.9	7.9	19.2
	Max =	6.7	15.0	32.4	105.7
	Min =	0.0	0.2	0.0	0.4

Comparing the results between both phantom materials, the absolute deviations are not significantly different ($p_{U,\rho_e} = 0.171$, $p_{U,Z_{eff}} = 0.923$).

3.4. Comparison with Bourque's method

Table 6 shows, for all samples, the descriptive statistics of the comparison in percent between the theoretical values and results of the stoichiometric methods. Using the Wilcoxon-Mann-Whitney U test for paired samples, the results of both methods are significantly different ($p_{U,\rho_e} = 0.008$; $p_{U,Z_{eff}} = 0.001$).

4. Discussion and conclusions

In this study, a method to calculate the electron density and effective atomic number for the results of a dual-energy CT is presented. The starting point is a representation of the attenuation coefficients. In this case a Karhunen-Loeve expansion with only one term is used. Only one term in the expansion gives an accurate representation of the attenuation coefficients as well as an effective atomic number independent of energy.

It is interesting to note the similarity between equation (4) (Midgley 2004), and the tissue functions in equation (13). In this work, the powers in atomic numbers are replaced by the orthogonal functions $f_i(Z)$.

In equation (14) the model was applied to composite tissues and equation (18) finally connects the model with the HU given by the CT. This connection was made through the parameters α_{HU} and β_{HU} which have been taken as free parameters, assuming that these parameters could deviate from their ideal values. This deviation seems to be confirmed by the lower energy of our CT, where the estimate of C_0 is significantly different from −1000.

The calibration was performed using the CIRS phantom and tested with independent samples prepared in our institution. These samples were not used in the calibration for two reasons: first, it may be easier for users to have a calibration phantom such as the CIRS phantom rather than samples whose composition is accurately known; and second, the authors believe that the CIRS phantom better mimics the dynamic range of variations of the ρ_e and Z_{eff} for human tissues.

The overall absolute differences, considering calibration and testing materials, are 1.7 % ± 0.1 % for the electron density and 4.1 % ± 0.3 % for the effective atomic number. These results are better than those obtained using Bourque's method and the differences are significant.

The CT used in this study is not a real dual-energy CT, i.e. it cannot provide the two sets of images in the same scan; nevertheless, the presented formalism should not change.

In this work, we used 80 and 140 kVp as the acceleration potentials, these are the minimum and maximum potentials provided by the CT used. It is expected that, with more dissimilar spectra, for example using 80–140/Sn kVp, the results obtained will be even better (Primak *et al* 2009).

Acknowledgments

The authors would like to thank the radiopharmacy laboratory of the Clínica Universidad de Navarra for the preparation of the samples and for help in calculating the element concentrations of those samples. The author would like to thank Santiago Pellejero from the Hospital de Navarra for his help in some aspects of this paper.

References

Bazalova M, Carrier J, Beaulieu L and Verhaegen F 2008a Dual-energy CT-based material extraction for tissue segmentation in Monte Carlo dose calculations *Phys. Med. Biol.* **53** 2439

Bazalova M, Carrier J, Beaulieu L and Verhaegen F 2008b Tissue segmentation in Monte Carlo treatment planning: a simulation study using dual-energy CT images *Radiother. Oncol.* **86** 93–8

Bornefalk H 2012 XCOM intrinsic dimensionality for low-Z elements at diagnostic energies *Med. Phys.* **39** 654–7

Bourque A E, Carrier J and Bouchard H 2014 A stoichiometric calibration method for dual energy computed tomography *Phys. Med. Biol.* **59** 2059

Buljak V 2011 *Inverse Analyses With Model Reduction: Proper Orthogonal Decomposition in Structural Mechanics* (Berlin: Springer)

De Levie R 2012 *Advanced Excel for Scientific Data Analysis* (Harpswell, ME: Atlantic Academic LCC)

Gerward L, Guilbert N, Jensen K B and Levring H 2004 WinXCom—a program for calculating x-ray attenuation coefficients *Radiat. Phys. Chem.* **71** 653–4

Heismann B, Leppert J and Stierstorfer K 2003 Density and atomic number measurements with spectral x-ray attenuation method *J. Appl. Phys.* **94** 2073–9

Hubbell J 1999 Review of photon interaction cross section data in the medical and biological context *Phys. Med. Biol.* **44** R1

Hyvärinen A, Karhunen J and Oja E 2004 *Independent Component Analysis* (New York: Wiley)

Jackson D F and Hawkes D J 1981 X-ray attenuation coefficients of elements and mixtures *Phys. Rep.* **70** 169–233

Landry G, Granton P V, Reniers B, Öllers M C, Beaulieu L, Wildberger J E and Verhaegen F 2011a Simulation study on potential accuracy gains from dual energy CT tissue segmentation for low-energy brachytherapy Monte Carlo dose calculations *Phys. Med. Biol.* **56** 6257

Landry G, Reniers B, Granton P V, van Rooijen B, Beaulieu L, Wildberger J E and Verhaegen F 2011b Extracting atomic numbers and electron densities from a dual source dual energy CT scanner: experiments and a simulation model *Radiother. Oncol.* **100** 375–9

Landry G, Seco J, Gaudreault M and Verhaegen F 2013 Deriving effective atomic numbers from DECT based on a parameterization of the ratio of high and low linear attenuation coefficients *Phys. Med. Biol.* **58** 19 6851

Liu X, Yu L, Primak A N and McCollough C H 2009 Quantitative imaging of element composition and mass fraction using dual-energy CT: three-material decomposition *Med. Phys.* **36** 1602–9

Midgley S 2004 A parameterization scheme for the x-ray linear attenuation coefficient and energy absorption coefficient *Phys. Med. Biol.* **49** 307

Pemler P, Schneider U and Besserer J 2001 Evaluation des Elektronendichte-Phantoms CIRS Model 62 *Z. Med. Phys.* **11** 25–32

Primak A, Giraldo J R, Liu X, Yu L and McCollough C 2009 Improved dual-energy material discrimination for dual-source CT by means of additional spectral filtration *Med. Phys.* **36** 1359–69

Saito M 2011 Optimized low-kV spectrum of dual-energy CT equipped with high-kV tin filtration for electron density measurements *Med. Phys.* **38** 2850–8

Saito M 2012 Potential of dual-energy subtraction for converting CT numbers to electron density based on a single linear relationship *Med. Phys.* **39** 2021–30

Saito M and Tsukihara M 2014 Technical note: exploring the limit for the conversion of energy-subtracted CT number to electron density for high-atomic-number materials *Med. Phys.* **41** 071701

Saito M 2015 Technical note: relation between dual-energy subtraction of CT images for electron density calibration and virtual monochromatic imaging *Med. Phys.* **42** 4088–93

Schneider W, Bortfeld T and Schlegel W 2000 Correlation between CT numbers and tissue parameters needed for Monte Carlo simulations of clinical dose distributions *Phys. Med. Biol.* **45** 459

Schneider U, Pedroni E and Lomax A 1996 The calibration of CT Hounsfield units for radiotherapy treatment planning *Phys. Med. Biol.* **41** 111

Seco J and Evans P 2006 Assessing the effect of electron density in photon dose calculations *Med. Phys.* **33** 540–52

Tsukihara M, Noto Y, Hayakawa T and Saito M 2013 Conversion of the energy-subtracted CT number to electron density based on a single linear relationship: an experimental verification using a clinical dual-source CT scanner *Phys. Med. Biol.* **58** N135

Tsukihara M, Noto Y, Sasamoto R, Hayakawa T and Saito M 2015 Initial implementation of the conversion from the energy-subtracted CT number to electron density in tissue inhomogeneity corrections: an anthropomorphic phantom study of radiotherapy treatment planning *Med. Phys.* **42** 1378–88

Wieser M E *et al* 2013 Atomic weights of the elements 2011 (IUPAC Technical Report) *Pure Appl. Chem.* **85** 1047–78

Williamson J F, Li S, Devic S, Whiting B R and Lerma F A 2006 On two-parameter models of photon cross sections: application to dual-energy CT imaging *Med. Phys.* **33** 11 4115–29

Zhang G, Cheng J, Zhang L, Chen Z and Xing Y 2008 A practical reconstruction method for dual energy computed tomography *J. X-Ray Sci. Technol.* **16** 67–88